PHYSICAL REVIEW D **86,** 094029 (2012)

Tagging single top quarks

Felix Kling, Tilman Plehn, and Michihisa Takeuchi
Institut für Theoretische Physik, Universität Heidelberg, 69120 Heidelberg, Germany
(Received 30 August 2012; published 19 November 2012)

Top taggers which identify and reconstruct boosted top quarks have been established as novel tools for a multitude of LHC analyses. We show how single top production in association with a light-flavor or bottom jet can be observed in the boosted phase space regime. The full top reconstruction as part of the tagging algorithm allows us to define a distinctive kinematic angle which clearly separates different single top production processes.

DOI: 10.1103/PhysRevD.86.094029 PACS numbers: 14.65.Ha

I. INTRODUCTION

Because of its large mass the top quark offers a unique handle on the structure of electroweak symmetry breaking and possible links to the origin of flavor. Its properties, like mass, charge, or W-helicity fractions, are mainly measured in top pair production with subsequent top decays [1–3]. The charged-current tbW coupling is directly accessible in single top production, i.e., without correlation to the remaining Cabibbo-Kobayashi-Maskawa mixing structure. The combined Tevatron analysis sets a lower limit on it as $V_{tb} > 0.77$ with 95% C.L., consistent with $V_{tb} = 1$ [4].

At the LHC we can study three different single top production modes: s-channel tb production via a timelike virtual W boson, t-channel tq production via a spacelike virtual W boson, and tW production in association with a real W boson. All of them should and will be separately measured, to test the electroweak properties of the heavy third quark generation. New physics contributions to the tbW coupling or to any of these three processes could be a first step to discover physics beyond the Standard Model (SM) [5–7]. General flavor-changing neutral current couplings, heavy W' gauge bosons, or a fourth generation are only a few examples.

In this context, it is worth noting that CDF reports a 2.5σ deviation from the Standard Model prediction in the ratio between s-channel and t-channel cross sections; only the sum of both channels agrees with the Standard Model predictions [8]. The corresponding D0 results are consistent with the Standard Model [9]. Recently, both experiments updated their results and are still inconsistent with each other at the 3σ level [10,11]. An improved understanding of single top production at the LHC seems in order.

The main difference between single top production at the Tevatron and at the LHC is that the s-channel production rate is significantly smaller than the t-channel rate at higher collider energies. This is because of the large gluon content in the proton which mainly enhances t-channel production (through $g \to b\bar{b}$ splitting) and tW production.

The relative size of the two different production rates strongly depends on the transverse momentum of the top quark. In Table I we show the different cross sections for top production with a variable minimum transverse momentum of the top quark. We gain a factor two for s-channel production relative to t-channel production when we focus on events with $p_{T,t} > 200$ GeV.

Measuring cross sections only in this boosted $p_{T,t}$ range provides independent information about single top production, in addition to the fully inclusive measurement. The left panel of Fig. 1 shows single top cross sections σ_s vs σ_t for all tops and for boosted tops only at 14 TeV (open circles) and at 8 TeV (filled circles). The CDF and D0 measurements together with the Standard Model prediction for the Tevatron are included for reference. The ratio of s-channel to t-channel cross sections becomes larger for boosted tops. The right panel of Fig. 1 shows the corresponding $p_{T,t}$ distributions for 14 TeV. Indeed, the s-channel curve drops slower than the other production channels. The only downside of the boosted regime is that the $t\bar{t}$ background is enhanced. This happens because $t\bar{t}$ production is mainly gluon-initiated and spin conservation suppresses the threshold regime.

In recent years, top tagging algorithms using jet substructure have rapidly matured [12–19]. A particularly efficient top tagging algorithm for moderately boosted hadronic tops is the HEPTOPTAGGER [20–24]. In this paper we investigate its possible benefit for single top searches in the fully hadronic decay mode. We will show that tagging boosted single tops allows us to overcome all backgrounds and extract both s-channel and t-channel single top production. Details of additional study can be found in Ref. [25].

II. EVENT GENERATION

Single top production accompanied with quarks can be categorized into

$$pp \to t\bar{b}\ (s\text{-channel}) \quad \text{and} \quad pp \to tq\ (t\text{-channel}), \tag{1}$$

plus the Hermitian conjugate final states. For t-channel production the possible final-state quarks can be $q = d$, s, $\bar{u}$, $\bar{c}$. We treat tW production as a background. To leading order, the two channels in Eq. (1) are obviously well

TABLE I. Top production cross sections for different minimum $p_{T,t}$ values for 8 TeV (left) and 14 TeV (right) center-of-mass energy. For $t\bar{t}$ we require at least one top exceeding the minimum $p_{T,t}$.

8 TeV: $p_{T,t}^{\min}$	0	100	200	300	400	500
σ_s [fb]	5548	1784	349	86.4	26.5	9.54
σ_t [fb]	86829	18167	2273	409.2	95.7	26.0
$\sigma_{t\bar{t}}$ [fb]	234731	137274	34640	7560	1850	519
σ_s/σ_t(%)	6.4	9.8	15.4	21.1	27.7	36.7
$\sigma_s/\sigma_{t\bar{t}}$(%)	2.36	1.29	1.00	1.14	1.43	1.83

14 TeV: $p_{T,t}^{\min}$	0	100	200	300	400	500
σ_s [fb]	11852	4206	964	292	108	43.8
σ_t [fb]	248194	59621	9128	2038	583	203
$\sigma_{t\bar{t}}$ [fb]	917935	572517	167564	43700	12771	4304
σ_s/σ_t(%)	4.7	7.0	10.5	14.3	18.5	21.5
$\sigma_s/\sigma_{t\bar{t}}$(%)	1.23	0.73	0.57	0.66	0.85	1.07

separated. Overlapping contributions of the kind $qg \to t\bar{b}q'$ do appear at next-to-leading order contributions to both processes. These are s-channel diagrams where one of the initial quarks is provided by gluon splitting, or t-channel diagrams where one of the initial b quarks arises through gluon splitting. They do not interfere because of different color flows; the $t\bar{b}$ system forms a color singlet for the s-channel process and a color octet for the t-channel. Hence, to next-to-leading order the two processes are well defined. Diagrams with additional gluons start interfering at next-to-next-to-leading order (NNLO) level. We consider this numerically irrelevant complication beyond the scope of our paper, even though in full QCD the separation of Eq. (1) should be reviewed.

As Standard Model backgrounds we consider $t\bar{t}$ + jets, QCD jets, W + jets, and tW production [26,27]. All corresponding samples are generated with Alpgen + Pythia [28,29]. For the signal with the very hard cuts (only) on the leading two constituents, leading order simulations with parton shower are sufficient. For all background processes other than tW we use MLM matching [30] to account for hard jet radiations. This includes up to $t\bar{t}$ + 2 jets, W + 4 jets, and 3–5 QCD jets. For tW production we combine tW and tWb samples and explicitly veto the phase space region $|m_{Wb} - m_t| < 5$ GeV overlapping with $t\bar{t}$ production (as recommended by ALPGEN). Eventually, we find that tW production is significantly suppressed compared to the $t\bar{t}$ background, so its simulation details do not affect our analysis.

All single top samples we then normalize to the approximate NNLO rates of 87.2 pb (t-channel), 5.55 pb (s-channel), and 22.2 pb (tW-channel) at 8 TeV [31]. Single top and antitop production in the s-channel contribute t: 3.79 pb and $\bar{t}$: 1.76 pb. For the t-channel we find t: 56.4 pb and $\bar{t}$: 30.7 pb, and for the tW-channel there is no preference for either charge. At 14 TeV LHC the rates become 11.86 pb (t: 7.87 pb and $\bar{t}$: 3.99 pb) for the s-channel, 248 pb (t: 154 pb and $\bar{t}$: 94 pb) for the t-channel, and 83.6 pb for

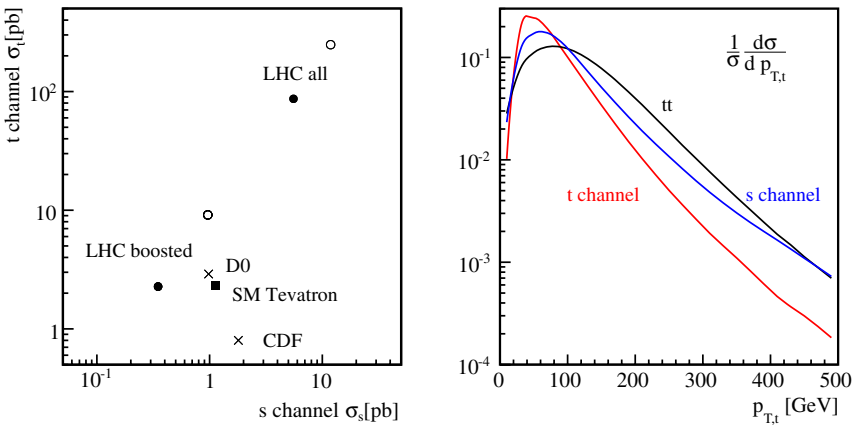

FIG. 1 (color online). Left: σ_s vs σ_t at the LHC. We show cross sections for inclusive single tops at the LHC, boosted tops ($p_{T,t} >$ 200 GeV) at the LHC, and the Tevatron. The open (filled) circles correspond to 14 TeV (8 TeV) results. Right: normalized $p_{T,t}$ distributions for s-channel and t-channel single top and $t\bar{t}$ at the 14 TeV LHC.

the tW-channel. The dominant $t\bar{t}+$jets background sample we normalize to the approximate NNLO rate of 234 pb (918 pb) for 8 TeV (14 TeV) [32]. For the remaining subleading background samples we use the leading order normalization.

Our detailed analysis includes DELPHES with default ATLAS detector setting as a fast detector simulation [33]. The calorimeter cell information provided by DELPHES is used as (fat)-jet constituents. As usual, we rely on the Cambridge/Aachen (C/A) algorithm [34] implemented in FASTJET [35]. The resulting fat jets defined with $R = 1.5$ are then used as input for the HEPTOPTAGGER [20,22]. The same C/A algorithm we use for regular QCD jets, but with $R = 0.5$. For regular well separated jets the algorithm should not matter, though. All leptons we require to be hard and isolated: $p_{T,\ell} > 10$ GeV and no track of another charged particle within $R < 0.5$ around the lepton, based on DELPHES. Triggering the hadronic single top events with highly energetic fat jets might or might not be a challenge, which we unfortunately have to leave to a more detailed experimental analysis.

III. SINGLE TOPS AT 8 TEV

In this section we discuss all selection cuts which we apply in our single top analyses and show results for t-channel and s-channel single top production at 8 TeV. We classify the set of cuts into three classes:

(1) cuts on the tagged top jet
(2) cuts on the balanced top and recoil jet system
(3) cuts on the recoil jet

A. Top tag

The starting point of our analysis is a balanced system of a fat top jet and its high-momentum recoil system. Hence, vetoing isolated leptons we first require two fat jets:

$$p_{T,\text{fat}} > 200 \text{ GeV}. \tag{2}$$

In those two fat jets we require exactly one top tag to avoid $t\bar{t}$ background. We use the HEPTOPTAGGER algorithm with modified parameters setting: the top mass window we slightly narrow to [160, 200] GeV instead of the default [150, 200] GeV. Similarly, we reduce the W mass window to $\pm 10\%$ instead of $\pm 15\%$, and increase the lower soft-collinear mass cut to $\arctan(m_{13}/m_{12}) > 0.45$ instead of 0.2. The tighter cuts reduce the top tagging efficiency but increase the fake-top rejection. It is necessary to obtain enough QCD rejection rate at the end as seen in Table II. Relative to the required two fat jets we now find a tagging efficiency of 12%–13% for signal events, and 16% for $t\bar{t}$ events. The latter is higher because there are two hadronic tops in each event but less than twice the single top efficiency because more events have two fat jets. The fake top rate for the QCD sample is about 1%, i.e., 0.5% per fat jet. The fake rate for $W+$ jets is about 3%. Both fake rates are based on the samples after requiring at least three jets with $R = 0.4$ in an event.

To extract the single top signal from the overwhelming QCD background we can use the pruned mass [22,36,37] in addition to the filtered mass [38]. Figure 2 shows their differences $\Delta m^{\text{prune}} = m^{\text{prune}} - m^{\text{filter}}$. We impose a cut

$$-10 < \Delta m^{\text{prune}} < 20 \text{ GeV}, \tag{3}$$

which is passed by about half of the events including tops and about 1/6 left for QCD jets. For the same purpose we then require a b tag inside the top tag. A b-tagging efficiency of 50% [39] translates into specific 40% inside the top tag, since the correct b-subjet selection ranges around 80% [22]. For QCD and $W+$ jets we assume a 1% fake rate.

In lines 0–4 of Table II we show the corresponding cut flow for signal and backgrounds. The set of cuts on the tagged top alone has an efficiency of 2%–3% for samples including tops and 1.5×10^{-5} for QCD relative to the number of events with two fat jets. Top pair production and QCD jets are the two main backgrounds at this stage.

B. Top-jet system: t-channel

Once the top is tagged we turn to the recoil jet which provides enough boost to the top. We ignore all calorimeter cells used for the constituents of the tagged top and cluster the remaining entries using the C/A jet algorithm with $R = 0.5$. We select the hardest jet as the (leading) recoil jet and require it to be above $p_{T,j} > 25$ GeV and inside the second fat jet. This way we define a reconstructed top momentum and its recoil.

TABLE II. Cut flow for the single top analysis at 8 TeV. The significances are quoted for t-channel single top production assuming all other processes as backgrounds.

8 TeV: Rates in fb	t-channel	s-channel	$t\bar{t}$	tW	QCD	$W+$ jets	S/B	$S/\sqrt{B_{10\ \text{fb}^{-1}}}$
0. Cross section	8.72×10^4	5.55×10^3	2.34×10^5	4.06×10^4	6.58×10^8	1.57×10^6	...	...
1. $n_\ell = 0$ with 2 fat jets [Eq. (2)]	1.57×10^3	230	1.88×10^4	1.63×10^3	6.67×10^6	4.81×10^4	0.0002	1.9
2. One top tag	204	28.2	3070	227	6.38×10^4	1297	0.003	2.5
3. Δm^{prune} cut [Eq. (3)]	110	13.9	1421	102	9.71×10^3	530	0.009	3.2
4. b tag in top tag	44.3	5.29	524	37.4	97.1	5.30	0.07	5.4
5. p_{tj} cut [Eq. (4)]	15.3	1.34	11.1	1.12	12.4	1.27	0.57	9.3
6. $\cos\theta^* < -0.5$ [Eq. (5)]	8.6	0.07	1.58	0.14	3.3	0.21	1.62	11.8

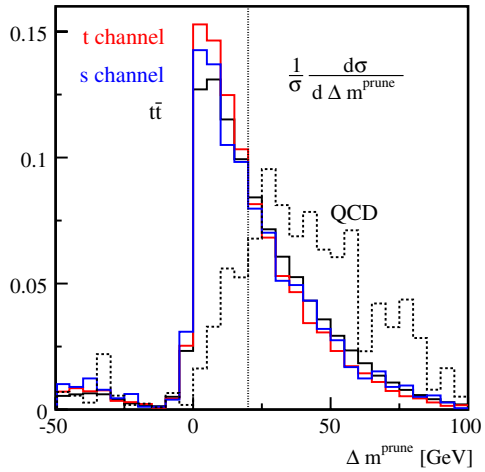

FIG. 2 (color online). Pruned-filtered mass difference Δm^{prune} distributions from the top tagger for the signal and the leading backgrounds.

The first variable we look at is the top-jet system momentum. The goal is to reject the leading $t\bar{t}$ background at this stage. Figure 3 shows the longitudinal vs the transverse system momentum for t-channel single top and $t\bar{t}$ production. We observe a distinct difference in their ratio: for the signal $p_{T,tj}$ tends to be small and $p_{L,tj}$ large while the opposite is true for top pairs. This can be understood for $t\bar{t}$ remembering that two pair-produced tops start off back-to-back, but the selected recoil jet often only includes part of the second top. The longitudinal system momentum is generally small for the dominant gluon fusion process. For the signal it can be understood by the unbalanced valence quark initial states.

Based on Fig. 3 we enhance the single top samples relative to top pairs by requiring

$$p_{T,tj} < \frac{p_{L,tj}}{60} + 10\ \text{GeV}. \tag{4}$$

This cut rejects up to 98% of the $t\bar{t}$ and tW backgrounds while keeping 35% of the signal. It is less effective against QCD (87%) but still helpful. This is because QCD events are dominated by dijets, one of which fakes the tagged top. The s-channel single top events behave similarly to the t-channel and survive to 25%. All results are shown in Table II.

As a side remark, the transverse component of the system momentum is similar to the Collins-Soper angle $\arctan(p_{T,tj}/m_{tj})$ [40]. Smaller $p_{T,tj}$ corresponds to a smaller Collins-Soper angle, but in our case the correlation between $p_{L,tj}$ and $p_{T,tj}$ appears to be the more powerful cut.

Initial-state parton combinations contribute differently to the different processes. The participating $b(\bar{b})$-parton density is even softer than for the other sea quarks; the system moves into the valence quark direction. Initial-state radiation affects this argument to some degree, but the main feature should be visible. Our second variable reflects this topology of single top Feynman diagrams and related kinematic enhancements. We define θ^* as the angle between (anti)top momentum in the rest frame of the tj system and the boost vector $\vec{\beta}$ from the rest frame to the laboratory frame. Many details on this angle are presented in the Appendix B.

Figure 4 shows the $\cos\theta^*$ distributions after all cuts to step 4 and to step 5 but without the cut on Δm^{prune}. We checked that this cut does not affect the shown distributions. The $\cos\theta^*$ distributions for single top production are reflecting the (polar) scattering angle distributions. This is because the direction of $\vec{\beta}$ follows the direction of the harder initial-state partons. For t-channel single top production with a qb initial state the top tends to be emitted in the direction of the b quark, corresponding to $\cos\theta^* \sim -1$. The same preference we expect from t-channel antitop production.

For s-channel single top production with a $u\bar{d}$ initial state the top tends to be emitted in the direction of the valence u quark, i.e., around $\cos\theta^* \sim 1$. The lower peak

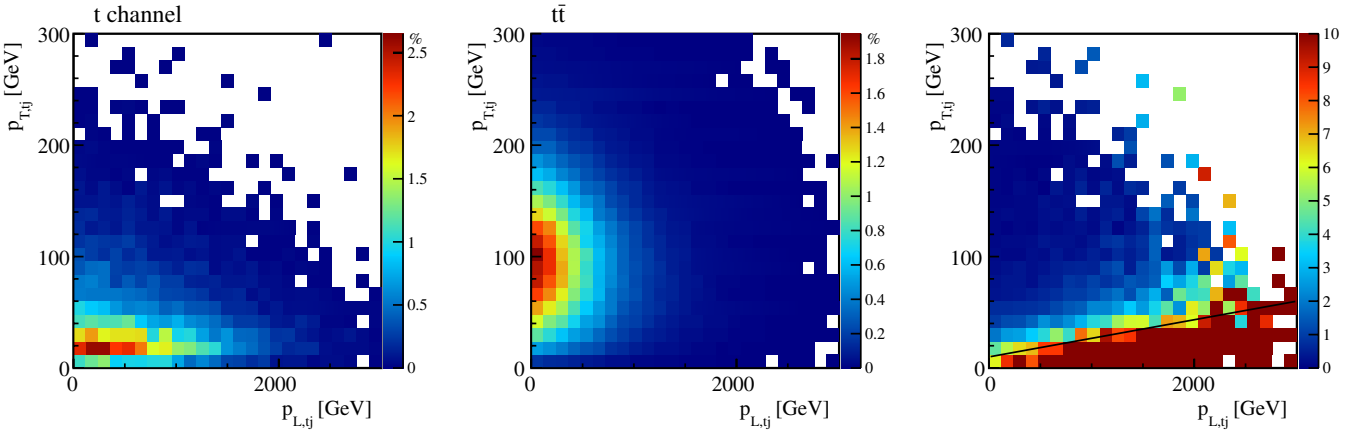

FIG. 3 (color online). $p_{L,tj}$ vs $p_{T,tj}$ distributions for t-channel single top production, $t\bar{t}$ production, and their ratio at 8 TeV.

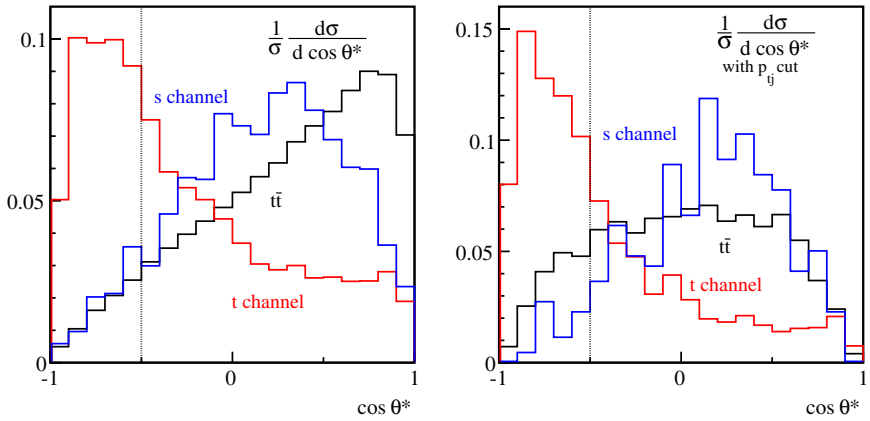

FIG. 4 (color online). Normalized $\cos\theta^*$ distributions before (left) and after (right) the p_{tj} cut for t-channel single top, s-channel single top, and top pair production at 8 TeV.

position can be understood from the decreasing top tagging efficiency once the top starts overlapping with the beam or has low $p_{T,t}$. For s-channel antitop production, $d\bar{u}$ is the main initial parton combination and it essentially results in the opposite $\cos\theta^*$ distribution. Provided that we cannot distinguish top charge in hadronic mode, the distribution we observe is combined distribution and contaminated by smaller antitop distribution.

The singly tagged top pair system moves toward the top direction, because usually the tj system only includes part of the second top as the assumed recoil. We indeed see a clear preference of large values $\cos\theta^* \sim 1$. Because this is the same reason as we already quoted for the transverse momentum balance of the tj system, this feature vanishes once we apply the cut Eq. (4). In the right panel of Fig. 4 the top pair distribution is essentially flat. Finally, for QCD there exists no clear correlation from the dijet topology.

We can turn this argument into the single top selection cut

$$\cos\theta^* < -0.5 \quad (t\text{-channel}). \tag{5}$$

As shown in Table II this cut leaves us with $S/B = 1.62$ and $S/\sqrt{B} > 10$ for 10 fb^{-1}. One might expect a b veto in the recoil as part of the t-channel single top search strategy, but since at this stage we are dominated by the pure QCD background we refrain from it.

C. Top recoil structure: s-channel

For the s-channel single tops we apply the same event selection as shown up to step 5 in Table II. The only difference is that the recoil jet is actually a central yet untagged bottom jet. In Fig. 4 we see that for s-channel single top production we should require

$$\cos\theta^* > -0.5 \quad (s\text{-channel}). \tag{6}$$

The numbers after successive cuts for s-channel search are summarized in Table III. The dominant backgrounds then are t-channel single top, $t\bar{t}$, and QCD jets.

The first additional cut on the recoil jet should obviously be a b tag. Because for top pairs the probability of identifying the b jet with the leading recoil jet is far from 100%, this cut is efficient also against the $t\bar{t}$ background. We again assume a 50% b-tagging efficiency and 1% fake rate. After this requirement, the t-channel single top, QCD, and W + jets backgrounds are under control.

To better reject the $t\bar{t}$ background we use the fact that the recoiling fat jet in single top production should be narrower and more isolated. For $t\bar{t}$ pairs the fat jet corresponding to the recoil jet often contains more than one subjet. To quantify this feature, we define the energy fraction of the filtered (leading) recoil jet inside the fat jet $E_j^{R<0.2}/E_{\text{fat}}$, where $E_j^{R<0.2}$ is the filtered energy of the recoil jet (with $R_{\text{filter}} = 0.2$ and $n_{\text{filter}} = 1$) and E_{fat} is the energy of the fat jet which contains the recoil jet. This

TABLE III. Cut flow for the s-channel single top analysis at 8 TeV. The significance values are quoted for s-channel single top production assuming all other channels as backgrounds and an integrated luminosity of 25 fb^{-1}.

8 TeV: Rates in fb	t-channel	s-channel	$t\bar{t}$	tW	QCD	W + jets	S/B	$S/\sqrt{B_{25\text{ fb}^{-1}}}$
1–5. One top tag, b tag, p_{tj} cut [Eq. (4)]	15.3	1.34	11.1	1.12	12.4	1.27	⋯	⋯
6. $\cos\theta^* > -0.5$ [Eq. (6)]	6.75	1.27	9.52	0.97	9.06	1.06	0.05	1.2
7. b tag in recoil jet	0.07	0.64	1.94	0.18	0.09	0.01	0.28	2.1
8. $E_j^{R<0.2}/E_{\text{fat}}$, $m_j < 65$ GeV [Eq. (7)]	0.04	0.35	0.11	0.02	0.03	⋯	1.75	3.9
9. $\not{p}_T < 40$ GeV [Eq. (8)]	0.04	0.32	0.07	0.02	0.03	⋯	2.00	4.0

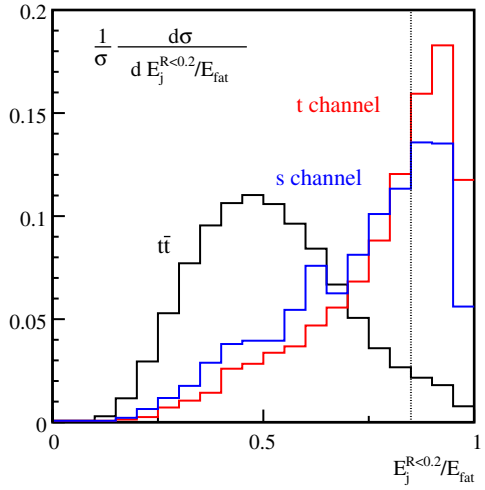

FIG. 5 (color online). $E_j^{R<0.2}/E_{\text{fat}}$ distributions for each process, as defined before Eq. (7).

condition is very similar to the usual lepton isolation criterion. Figure 5 shows the $E_j^{R<0.2}/E_{\text{fat}}$ distributions. Top pairs indeed lead to a softer distribution, not peaked at unity. Hence, we require

$$\frac{E_j^{R<0.2}}{E_{\text{fat}}} > 0.85 \quad \text{and} \quad m_j < 65\ \text{GeV}, \tag{7}$$

where m_j is the jet mass of the recoil jet. Recoil jets consistent with a boosted W decay are also removed by the second condition $m_j < 65$ GeV, even though the fraction is not large. This cut reduces $t\bar{t}$ events to roughly 5% while keeping half of the signal. We also considered a cut on E_j/E_{fat} without filtering instead, but it gives a weaker background suppression.

At this stage, a part of $t\bar{t}$ background consists of events with a leptonic (e, μ, τ) top decay. This means it includes large missing momentum which we can use to require

$$\not{p}_T < 40\ \text{GeV}. \tag{8}$$

Combining all sets of the cuts s-channel signal analysis for 8 TeV LHC results in $S/B = 2.0$ and $S/\sqrt{B} = 4.0$ for 25 fb^{-1}.

IV. SINGLE TOPS AT 14 TEV

Following our results for the 8 TeV LHC run we study the same two signatures for 14 TeV collider energy. Because our analysis relies on boosted and hence fairly energetic tops we expect significant improvements from this energy increase. All relevant cross sections are of course larger. Following Table I the boosted top cross sections increase by roughly a factor 3 for s-channel single top production, 4 for the t-channel, and 5 for $t\bar{t}$. This implies that there will be a tradeoff between S/B and the significance from an improved boosted regime.

First, we present the results for t-channel single top production. Table IV shows the rates after all cuts described in the previous section. Asking for exactly one top tag for events with two fat jets we find an efficiency around 12% for the single top samples, 15% for top pairs, and around 1% for QCD. These values are almost the same as for 8 TeV. Next, we cut on the top tag, namely, the pruned mass given in Eq. (3) and a b-tag. We find an efficiency around 20% for the signal, 16% for top pairs, 0.12% for QCD, and 0.3% for W + jets. Again, there are no big changes from the 8 TeV analysis.

After applying the tj-system momentum cut of Eq. (4), the signal rate is of similar order as the leading backgrounds. Selecting events with $\cos\theta^* < -0.5$, we can extract t-channel single top production with $S/B = 1.7$. Finally, we cut on the recoil jet system, Eq. (7), and arrive at $S/B \sim 3$ and a promising signal significance, indeed.

For the s-channel single top search we need to check that the enhanced $t\bar{t}$ background does not pose a major problem at 14 TeV. Following Table I the naive signal-to-background estimate otherwise drops by almost a factor two. The efficiencies of the same successive 8 TeV cuts on 14 TeV events we show in Table V. After selecting $\cos\theta^* > -0.5$ and requiring a b-tagged leading recoil jet we are left with 2 fb of signal rate with a six times larger $t\bar{t}$ background.

After applying all selection cuts, a 0.95 fb s-channel single top signal is left with the same amount of background mainly from $t\bar{t}$ and QCD. As expected, the signal cross section at this stage is three times the 8 TeV result while the $t\bar{t}$ background is six times the value quoted in Table III. We achieve $S/B = 1.13$ and $S/\sqrt{B} = 5.2$ for

TABLE IV. Cut flow for the t-channel single top analysis at 14 TeV. The significance is computed based on the statistical error for 10 fb^{-1}.

14 TeV: Rates in fb	t-channel	s-channel	$t\bar{t}$	tW	QCD	W + jets	S/B	$S/\sqrt{B_{10\,\text{fb}^{-1}}}$
0. Cross section	2.48×10^5	1.18×10^4	9.20×10^5	1.60×10^5	1.94×10^9	3.88×10^6	0.0003	...
1. $n_\ell = 0$ with 2 fat jets [Eq. (2)]	6590	670	9.53×10^4	1.02×10^4	2.83×10^7	1.29×10^5	0.0004	...
2. One top tag	819	81.4	1.48×10^4	1350	3.00×10^5	3015	0.003	4.6
3. Δm^{prune} cut [Eq. (3)]	416	40.4	6438	578	3.61×10^4	1005	0.009	6.3
4. b tag	166	15.5	2346	212	361	10.1	0.06	9.7
5. p_{tj} cut [Eq. (4)]	67.8	4.28	72.7	9.20	75.5	2.53	0.41	16.7
6. $\cos\theta^* < -0.5$ [Eq. (5)]	41.2	0.30	14.6	1.18	7.15	0.55	1.74	26.8
7. $E_j^{R<0.2}/E_{\text{fat}}$, $m_j < 65$ GeV [Eq. (7)]	36.1	0.25	7.33	0.50	3.58	0.50	2.97	32.7

TABLE V. Cut flow for the s-channel single top analysis at 14 TeV. The significance assumes 25 fb^{-1} with all other channels being backgrounds.

14 TeV: rates in fb	t-channel	s-channel	$t\bar{t}$	tW	QCD	W + jets	S/B	$S/\sqrt{B_{25\,\mathrm{fb}^{-1}}}$
1–5. one top tag, b tag, p_{tj} cut [Eq. (4)]	67.8	4.28	72.7	9.20	75.5	2.53	···	···
6. $\cos\theta^* > -0.5$ [Eq. (6)]	26.6	3.99	58.2	8.02	68.3	1.99	0.02	1.6
7. b tag in recoil jet	0.27	1.99	12.6	0.76	0.68	0.02	0.14	2.6
8. $E_j^{R<0.2}/E_{\mathrm{fat}}$, $m_j < 65$ GeV [Eq. (7)]	0.15	1.00	0.75	0.08	0.26	···	0.80	4.5
9. $\not{p}_T < 40$ GeV [Eq. (8)]	0.14	0.95	0.41	0.03	0.26	···	1.13	5.2

25 fb^{-1}. The signal-to-background ratio can be improved at the expense of the significance simply by tightening the different cuts.

V. CONCLUSIONS

Using the HEPTOPTAGGER single top production in the purely hadronic channel can be observed at the LHC. Controlling the $t\bar{t}$ and QCD background is the key to these single top searches. By applying successive cuts on the tagged top jet and the fully reconstructed top and recoil system, we achieve $S/B > 1$ with $S/\sqrt{B} > 10$ for the t-channel process at 8 TeV with 10 fb^{-1}. For this result we need to gain a factor 10 against top pairs and a factor 4000 against QCD jets after selecting events with two fat jets. Most of this is provided by the top tag. Additional cuts on the recoil jet, including a b tag and a cut on the size of the recoil jet, can extract the s-channel with 4 sigma and $S/B > 1$ at the same energy with an integrated luminosity of 25 fb^{-1}. To distinguish the two single top production modes and to reject backgrounds we introduce a new angular observable θ^* which is highly efficient once we reconstruct the top momentum.

For the 14 TeV we can use the same analysis. The signal-to-background ratios are similar to the 8 TeV case for the t-channel and slightly worse than the 8 TeV result for the s-channel. Thanks to the larger cross sections the significance exceeds 5σ even for the s-channel process with an integrated luminosity of 25 fb^{-1}.

ACKNOWLEDGMENTS

We would like to thank Michael Spannowsky and all colleagues who have continuously helped to develop and improve the HEPTOPTAGGER. The Heidelberg ATLAS group and Dirk Zerwas we would like to thank for their help with detector effects and their simulation.

APPENDIX A: DETECTOR EFFECTS

In this appendix we summarize the effects of the fast detector simulation DELPHES on the performance of the HEPTOPTAGGER. In the left two panels of Fig. 6 we show the top mass and the W mass distributions reconstructed in the t-channel top sample. Both are slightly smeared out by detector effects, just as expected. The top mass and W mass peak positions do not shift significantly. As long as the mass ranges required by the top tagger are sufficiently large, the tagging efficiency should not change. In particular, the mass ranges assumed in Sec. III A should be conservative.

The right panel of Fig. 6 shows the difference between the pruned mass [36] and the filtered mass [38] ($\Delta m^{\mathrm{prune}} = m^{\mathrm{prune}} - m^{\mathrm{filter}}$) with and without detector effects. This distribution is smeared out significantly and shifted toward larger values. Hence, this additional observable introduced in Ref. [22] requires an experimental study and validation.

Figure 7 shows how well the top tagger reconstructs the top momentum. Detailed particle-level results including the

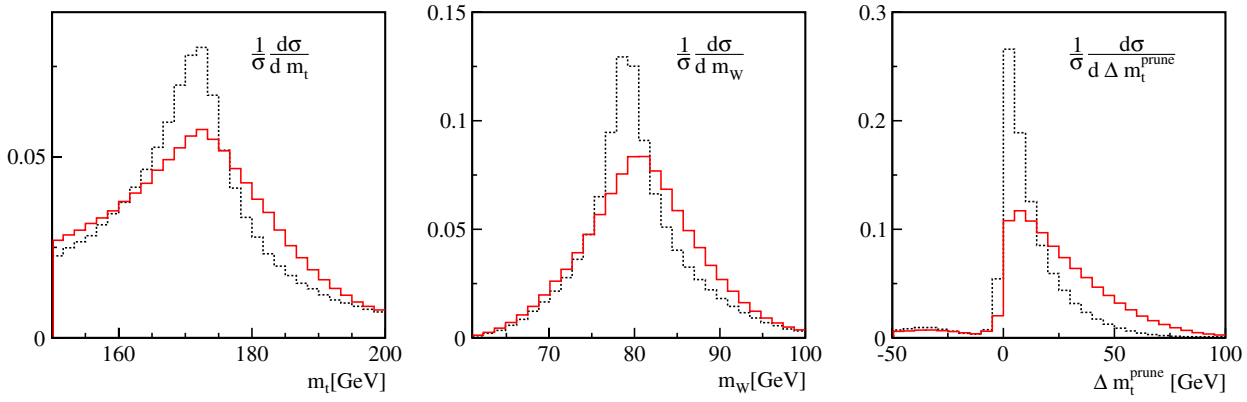

FIG. 6 (color online). Top tagging observables m_t, m_W, and m_t^{prune} for the t-channel single top sample with (solid red) and without DELPHES (dashed black).

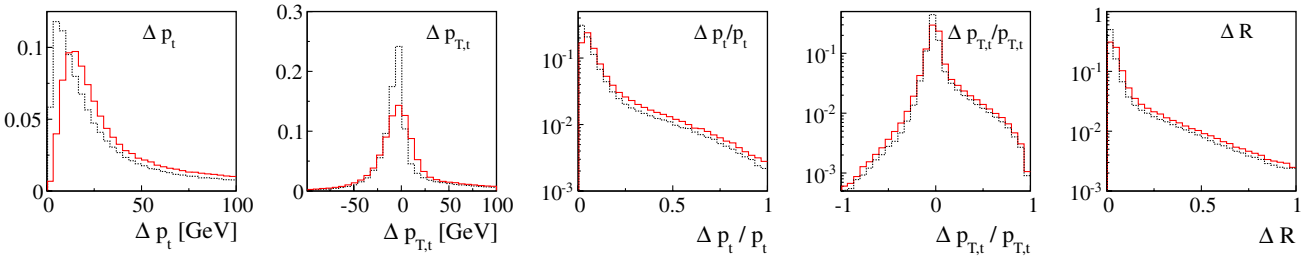

FIG. 7 (color online). From left to right, the Δp_t, $\Delta p_{T,t}$, $\Delta p_t/|p_t^{\text{tag}}|$, $\Delta p_{T,t}/p_{T,t}^{\text{tag}}$, and ΔR distribution for the t-channel single top sample, shown with (solid red) and without DELPHES (dashed black).

quality of the actual tagging algorithm can be found in Ref. [22]. In this appendix we focus on its DELPHES simulation. We show, from left to right, $\Delta p_t = |\mathbf{p}_t^{\text{tag}} - \mathbf{p}_t|$, $\Delta p_{T,t} = p_{T,t}^{\text{tag}} - p_{T,t}$, $\Delta p_t/|p_t^{\text{tag}}|$, $\Delta p_{T,t}/p_{T,t}^{\text{tag}}$, and ΔR. We see slight smearing but no significant qualitative difference. Most tagged tops are reconstructed within an error bar of $\Delta R < 0.2$ and within a 15% error in the momentum p_t.

APPENDIX B: TOP-JET ANGLES

The search for single tops using a top tagger has a significant advantage: once the tagger has identified a top jet we automatically get a full momentum reconstruction of this top quark. As described in the previous appendix this 4-momentum reconstruction is quite accurate. The obvious challenge is to define appropriate angular variables which allow us to distinguish between s-channel and t-channel single top production and the top pair background, respectively.

For t-channel production the hard partonic process is $qb \to q't$. Here, $q(q')$ denotes possible initial (final) (anti) quarks of the first and second generations. Assuming (unrealistic) full control over the initial and final states we define θ as the angle between the top direction t and the incoming quark direction q in the center-of-mass frame, i.e., the scattering angle of the hard subprocess. The differential cross section with fixed center-of-mass energy squared s gives its distribution

$$\frac{d\sigma_t}{d\cos\theta} \propto \frac{1}{\left(1 + \cos\theta + \frac{2m_W^2}{s - m_t^2}\right)^2}, \tag{B1}$$

with a maximum at $\cos\theta = -1$ or $\theta = \pi$. This means the top prefers to follow the direction of the incoming bottom, i.e., opposite to the incoming quark q. This is typical for t-channel processes. Note that for antitop production $q\bar{b} \to \bar{t}q'$ we define θ as the angle between the $\bar{t}$ and the incoming quark q and obtain the same angular distribution through charge conjugation.

For s-channel production $u\bar{d} \to t\bar{b}$ we define θ as the angle between the top direction and the incoming u quark. The differential cross section is

$$\frac{d\sigma_s}{d\cos\theta} \propto \frac{2m_t^2(1 + \cos\theta) + s\left(1 - \frac{m_t^2}{s}\right)(1 + \cos\theta)^2}{s - m_W^2}. \tag{B2}$$

The distribution has a maximum at $\cos\theta = 1$ or $\theta = 0$; i.e., the top tends to be emitted in the incoming u-quark direction. For antitop production $d\bar{u} \to \bar{t}b$ we define θ as the angle between the antitop and the incoming $\bar{u}$ and obtain the same angular distribution through charge conjugation.

The leftmost panel of Fig. 9 shows the above distributions as functions of $\cos\theta$ with fixed $\sqrt{s} = 500$ GeV. In the central panel we see the same distributions, now folded with parton densities and with an explicit $p_{T,t}$ cut, $p_{T,t} > 200$ GeV. A loss of the events around $\cos\theta \sim \pm 1$ can be observed. Note that cuts on $p_{T,t}$ and $\cos\theta$ are linked because of the leading order kinematic relation $p_T = (\sqrt{s}/2)|\cos\theta|$.

Unfortunately, the angle θ cannot be extracted at the LHC event by event. Therefore, we define the modified angle θ^* between the top direction in the rest frame of the top plus recoil jet system and the direction of $\vec{\beta}$, describing the boost from the rest frame to the laboratory frame, as seen in Fig. 8. This boost lies mostly in the direction of the incoming beams and reflects the difference in the partonic momentum fractions of the two incoming (anti)quarks. The behavior of θ^* closely tracks the above described angle θ.

For t-channel single tops the boost vector is preferably pointed in the initial quark direction, because incoming

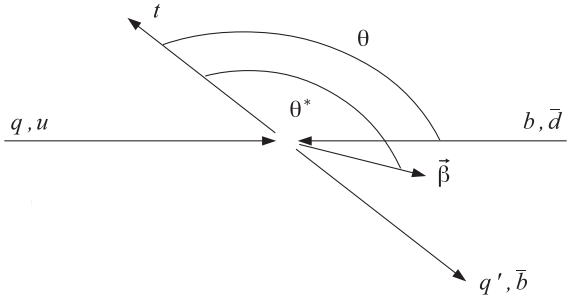

FIG. 8. Kinematics of single top production in the s- and t-channel with the definition of the angles $\cos\theta$ and $\cos\theta^*$.

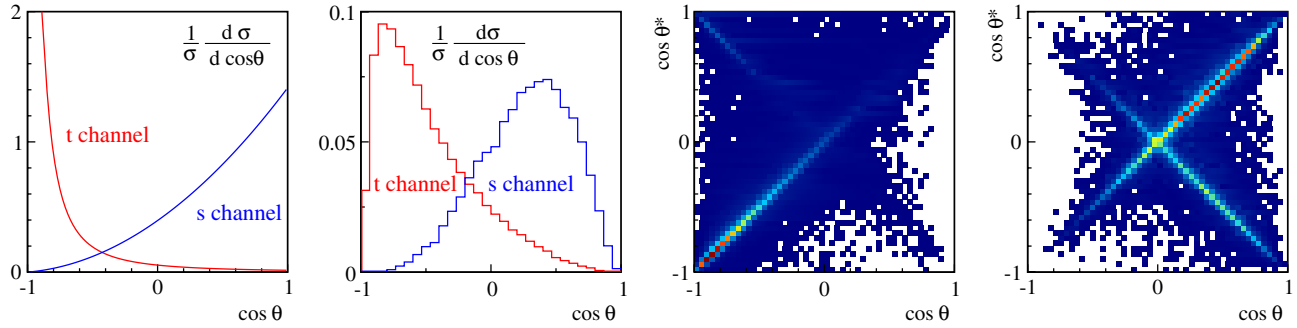

FIG. 9 (color online). From the left: normalized $d\sigma_t/d\cos\theta$ and $d\sigma_s/d\cos\theta$ for a fixed partonic energy $\sqrt{s} = 500$ GeV; normalized $d\sigma_t/d\cos\theta$ and $d\sigma_s/d\cos\theta$ for single top events with $p_{T,t} > 200$ GeV; $\cos\theta$ vs $\cos\theta^*$ for t-channel single top production; the same for s-channel single top production. The dense region is shown in red (light gray).

bottom partons have significantly softer partonic energy spectra. Therefore, the $\cos\theta^*$ distribution essentially reproduces the $\cos\theta$ distribution as shown in Fig. 4. This relation for the t-channel single top sample at the parton level is shown in the third panel of Fig. 9. We see a clear preference for $\cos\theta^* = \pm\cos\theta$, where the more likely relative plus sign appears when the incoming quark is more energetic than the incoming bottom. Note that it is also true for t-channel antitop production. The same correlation appears for the s-channel single top sample as seen in the most right panel of Fig. 9, while more minus signs appear due to antitop single production.

[1] Tevatron Electroweak Working Group, CDF, and D0 Collaborations, arXiv:1107.5255.

[2] V. M. Abazov *et al.* (D0 Collaboration), Phys. Rev. Lett. **98**, 041801 (2007); CDF Collaboration, Report No. 10460, http://www-cdf.fnal.gov/physics/new/top/2011/topQLJ/cdf10460_topq_56invfb.pdf.

[3] T. Aaltonen *et al.* (CDF and D0 Collaborations), Phys. Rev. D **85**, 071106 (2012); T. Aaltonen *et al.* (CDF Collaboration), Phys. Rev. Lett. **105**, 042002 (2010); V. M. Abazov *et al.* (D0 Collaboration), Phys. Rev. D **83**, 032009 (2011).

[4] T. E. W. Group, CDF, and D0 Collaborations, arXiv:0908.2171.

[5] T. M. P. Tait and C.-P. Yuan, Phys. Rev. D **63**, 014018 (2000).

[6] J. Alwall, R. Frederix, J.-M. Gerard, A. Giammanco, M. Herquet, S. Kalinin, E. Kou, V. Lemaitre, and F. Maltoni, Eur. Phys. J. C **49**, 791 (2007).

[7] D. E. Morrissey, T. Plehn, and T. M. P. Tait, Phys. Rep. **515**, 1 (2012).

[8] T. Aaltonen *et al.* (CDF Collaboration), Phys. Rev. Lett. **103**, 092002 (2009); Phys. Rev. D **82**, 112005 (2010).

[9] V. M. Abazov *et al.* (D0 Collaboration), Phys. Rev. Lett. **103**, 092001 (2009); Phys. Lett. B **682**, 363 (2010); Phys. Rev. D **84**, 112001 (2011).

[10] CDF Collaboration, Report No. 10793, http://www-cdf.fnal.gov/physics/new/top/confNotes/cdf10793_SingleTop_7.5_public.pdf.

[11] V. M. Abazov *et al.* (D0 Collaboration), Phys. Lett. B **705**, 313 (2011).

[12] J. Thaler and L.-T. Wang, J. High Energy Phys. 07 (2008) 092; D. Krohn, J. Thaler, and L.-T. Wang, J. High Energy Phys. 06 (2009) 059; 02 (2010) 084.

[13] I. W. Stewart, F. J. Tackmann, and W. J. Waalewijn, Phys. Rev. Lett. **105**, 092002 (2010); J.-H. Kim, Phys. Rev. D **83**, 011502 (2011); J. Thaler and K. Van Tilburg, J. High Energy Phys. 02 (2012) 093; S. D. Ellis, A. Hornig, T. S. Roy, D. Krohn, and M. D. Schwartz, Phys. Rev. Lett. **108**, 182003 (2012).

[14] D. E. Kaplan, K. Rehermann, M. D. Schwartz, and B. Tweedie, Phys. Rev. Lett. **101**, 142001 (2008); K. Rehermann and B. Tweedie, J. High Energy Phys. 03 (2011) 059; I. Feige, M. Schwartz, I. Stewart, and J. Thaler, Phys. Rev. Lett. **109**, 092001 (2012).

[15] L. G. Almeida, S. J. Lee, G. Perez, G. F. Sterman, I. Sung, and J. Virzi, Phys. Rev. D **79**, 074017 (2009); L. G. Almeida, S. J. Lee, G. Perez, I. Sung, and J. Virzi, Phys. Rev. D **79**, 074012 (2009); L. G. Almeida, S. J. Lee, G. Perez, G. Sterman, and I. Sung, Phys. Rev. D **82**, 054034 (2010).

[16] A. Hook, M. Jankowiak, and J. G. Wacker, J. High Energy Phys. 04 (2012) 007; M. Jankowiak and A. J. Larkoski, J. High Energy Phys. 06 (2011) 057; 04 (2012) 039.

[17] G. Brooijmans, Report No. ATL-PHYS-CONF-2008-008; CMS Collaboration, Report No. CMS-PAS-JME-10-013.

[18] A. Abdesselam *et al.*, Eur. Phys. J. C **71**, 1661 (2011); A. Altheimer *et al.*, J. Phys. G **39**, 063001 (2012).

[19] For a pedagogical overview of top tagger see, e.g., T. Plehn and M. Spannowsky, J. Phys. G **39**, 083001 (2012).

[20] T. Plehn, G. P. Salam, and M. Spannowsky, Phys. Rev. Lett. **104**, 111801 (2010); T. Plehn, M. Spannowsky,

M. Takeuchi, and D. Zerwas, J. High Energy Phys. 10 (**2010**) 078; http://www.thphys.uni-heidelberg.de/~plehn.
[21] T. Plehn, M. Spannowsky, and M. Takeuchi, J. High Energy Phys. 05 (2011) 135.
[22] T. Plehn, M. Spannowsky, and M. Takeuchi, Phys. Rev. D **85**, 034029 (2012).
[23] T. Plehn, M. Spannowsky, and M. Takeuchi, J. High Energy Phys. 08 (2012) 091.
[24] ATLAS Collaboration, Report No. ATLAS-CONF-2012-065, https://atlas.web.cern.ch/Atlas/GROUPS/PHYSICS/CONFNOTES/ATLAS-CONF-2012-065.
[25] F. Kling, Master's thesis, Universität Heidelberg, http://www.thphys.uni-heidelberg.de/~plehn/includes/theses/kling.pdf.
[26] G. Aad *et al.* (ATLAS Collaboration), arXiv:1205.3130; Phys. Lett. B **716**, 142 (2012).
[27] S. Chatrchyan *et al.* (CMS Collaboration), Phys. Rev. Lett. **107**, 091802 (2011).
[28] M. L. Mangano, M. Moretti, F. Piccinini, R. Pittau, and A. D. Polosa, J. High Energy Phys. 07 (2003) 001.
[29] T. Sjostrand, S. Mrenna, and P. Z. Skands, J. High Energy Phys. 05 (2006) 026; Comput. Phys. Commun. **178**, 852 (2008).
[30] M. L. Mangano, M. Moretti, F. Piccinini, and M. Treccani, J. High Energy Phys. 01 (2007) 013.
[31] N. Kidonakis, Phys. Rev. D **81**, 054028 (2010); **83**, 091503 (2011); **82**, 054018 (2010).
[32] N. Kidonakis, Phys. Rev. D **82**, 114030 (2010); V. Ahrens, A. Ferroglia, M. Neubert, B. D. Pecjak, and L. L. Yang, Phys. Lett. B **703**, 135 (2011); M. Cacciari, M. Czakon, M. L. Mangano, A. Mitov, and P. Nason, Phys. Lett. B **710**, 612 (2012); S. Moch, P. Uwer, and A. Vogt, Phys. Lett. B **714**, 48 (2012).
[33] S. Ovyn, X. Rouby, and V. Lemaitre, arXiv:0903.2225.
[34] Y. L. Dokshitzer, G. D. Leder, S. Moretti, and B. R. Webber, J. High Energy Phys. 08 (1997) 001; M. Wobisch and T. Wengler, arXiv:hep-ph/9907280.
[35] M. Cacciari and G. P. Salam, Phys. Lett. B **641**, 57 (2006); M. Cacciari, G. P. Salam, and G. Soyez, Eur. Phys. J. C **72**, 1896 (2012); http://fastjet.fr.
[36] S. D. Ellis, C. K. Vermilion, and J. R. Walsh, Phys. Rev. D **80**, 051501 (2009).
[37] D. E. Soper and M. Spannowsky, J. High Energy Phys. 08 (2010) 029.
[38] J. M. Butterworth, A. R. Davison, M. Rubin, and G. P. Salam, Phys. Rev. Lett. **100**, 242001 (2008).
[39] G. Piacquadio and U. Freiburg, Report No. CERN-THESIS-2010-027.
[40] J. C. Collins and D. E. Soper, Phys. Rev. D **16**, 2219 (1977); T. Plehn, M. Rauch, and M. Spannowsky, Phys. Rev. D **80**, 114027 (2009).